



Alkyne-tagged PLGA allows direct visualisation of nanoparticles in vitro and ex vivo by stimulated Raman scattering microscopy

DOI:

[10.1021/acs.biomac.9b01092](https://doi.org/10.1021/acs.biomac.9b01092)

[Link to publication record in Manchester Research Explorer](#)

Citation for published version (APA):

Vanden-hehir, S., Cairns, S. A., Lee, M., Zoupi, L., Shaver, M. P., Brunton, V. G., Williams, A., & Hulme, A. N. (2019). Alkyne-tagged PLGA allows direct visualisation of nanoparticles in vitro and ex vivo by stimulated Raman scattering microscopy. *Biomacromolecules*. Advance online publication. <https://doi.org/10.1021/acs.biomac.9b01092>

Published in:

Biomacromolecules

Citing this paper

Please note that where the full-text provided on Manchester Research Explorer is the Author Accepted Manuscript or Proof version this may differ from the final Published version. If citing, it is advised that you check and use the publisher's definitive version.

General rights

Copyright and moral rights for the publications made accessible in the Research Explorer are retained by the authors and/or other copyright owners and it is a condition of accessing publications that users recognise and abide by the legal requirements associated with these rights.

Takedown policy

If you believe that this document breaches copyright please refer to the University of Manchester's Takedown Procedures [<http://man.ac.uk/04Y6Bo>] or contact openresearch@manchester.ac.uk providing relevant details, so we can investigate your claim.



1
2
3
4
5
6
7 Alkyne-tagged PLGA allows direct visualisation of
8
9
10
11 nanoparticles *in vitro* and *ex vivo* by stimulated
12
13
14
15 Raman scattering microscopy
16
17
18
19

20 *Sally Vanden-Hehir*^a, *Stefan A. Cairns*^a, *Martin Lee*^b, *Lida Zoupi*^c, *Michael Patrick*

21
22
23
24 *Shaver*^{a†}, *Valerie G. Brunton*^b, *Anna Williams*^c and *Alison Nicola Hulme*^{a*}
25
26
27

28 ^aEaStCHEM School of Chemistry, University of Edinburgh, David Brewster Road,
29
30

31
32 Edinburgh, EH9 3FJ, UK
33
34
35

36 ^bEdinburgh Cancer Research Centre, University of Edinburgh, Western General
37
38

39
40 Hospital, Crewe Road South, Edinburgh, EH4 2XR, UK
41
42
43

44 ^cMRC Centre for Regenerative Medicine, The University of Edinburgh, Edinburgh
45
46

47
48 BioQuarter, 5, Little France Drive, Edinburgh, EH16 4UU, UK
49
50

51 1
52
53
54
55
56
57
58
59
60

1
2
3
4 ABSTRACT
5
6
7

8 Polymeric nanoparticles (NPs) are attractive candidates for the controlled and targeted
9
10 delivery of therapeutics *in vitro* and *in vivo*. However, detailed understanding of the
11
12 uptake, location and ultimate cellular fate of the NPs is necessary in order to satisfy
13
14 safety concerns, which is difficult because of the nanoscale size of these carriers. In this
15
16 work, we show how small chemical labels can be appended to poly(lactic acid-*co*-
17
18 glycolic acid) (PLGA) in order to synthesise NPs that can then be imaged by stimulated
19
20 Raman scattering (SRS) microscopy, a vibrational imaging technique which can
21
22 elucidate bond specific information in biological environments, such as the identification
23
24 of alkyne signatures in modified PLGA terpolymers. We show that both deuterium and
25
26 alkyne labelled NPs can be imaged within primary rat microglia, and the alkyne NPs can
27
28 also be imaged *ex vivo* cortical mouse brain tissue. Immunohistochemical analysis
29
30
31
32
33
34
35
36
37
38
39
40
41
42
43
44
45
46
47
48
49
50
51
52
53
54
55
56
57
58
59
60

1
2
3 confirms that the NPs localize in microglia in the mouse brain tissue, demonstrating that
4
5
6
7 these NPs have the potential to deliver therapeutics selectively to microglia.
8
9

10 11 KEYWORDS

12
13
14
15 Nanoparticles, drug delivery, alkynes, Raman imaging, bioorthogonal polymers,
16
17
18
19 stimulated Raman scattering
20
21
22
23
24
25

26 27 INTRODUCTION

28
29
30
31 The use of polymeric NPs for drug delivery has become increasingly popular in order to
32
33
34 achieve controlled release, targeted delivery and increased lifetime of therapeutics *in*
35
36
37
38 *vivo*. NP drug delivery can have wide ranging applications such as the targeting of
39
40
41 cancer therapeutics,^{1,2} delivery of drugs to the brain,^{3,4} and encapsulation protein
42
43
44
45 therapeutics, which are sensitive to certain biological environments and may degrade to
46
47
48 an inactive form *in vivo*. PLGA micro and nanoparticles have been used extensively in
49
50

51 3
52
53
54
55
56
57
58
59
60

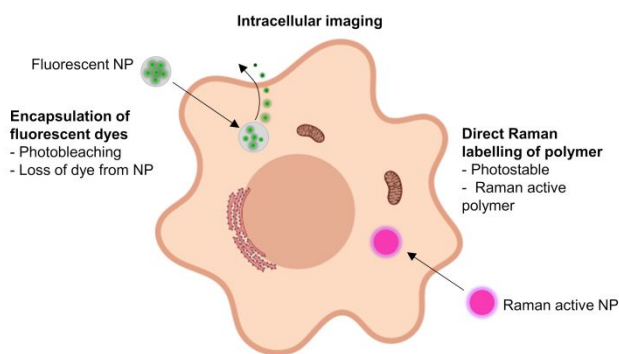
1
2
3 drug delivery research as they are FDA approved, biocompatible and biodegradable.⁵
4
5

6
7 However, due to the nanoscale size of these drug carriers, imaging their uptake, bio-
8
9
10 distribution and ultimate cellular fate *in vitro* and *in vivo* is challenging.
11
12

13
14 Previous efforts to image polymer NPs have mainly focused on the encapsulation of
15
16
17
18 fluorescent dyes inside the NPs to allow imaging by fluorescence microscopy,⁶ or by
19
20
21 various Raman-based methods, which we have recently reviewed.⁷ The degradation of
22
23
24
25 PLGA NPs in macrophages has been monitored by quantifying the loss of fluorescent
26
27
28
29 signal over time.⁸ PLGA NPs degrade by hydrolysis under physiological conditions,⁹
30
31
32 thus the loss of fluorescent signal could correspond to dye being released from the NPs,
33
34
35
36 and not give direct information about the location and state of the NP. Also,
37
38
39
40 fluorophores are generally unstable in biological environments, and photobleaching can
41
42
43 also cause signal degradation of the dye (Figure 1).¹⁰
44
45
46
47
48
49
50

51 4
52
53
54
55
56
57
58
59
60

1
2
3 Stimulated Raman scattering (SRS) microscopy has emerged as a powerful, label-free
4
5
6
7 optical imaging technique for biological systems that can provide quantitative and bond-
8
9
10 specific cellular information.^{11,12} Spontaneous Raman scattering can be used to probe
11
12
13 the chemical signature of cells and biological tissues due to the inelastic scattering of
14
15
16
17 light when the sample is irradiated with a laser, but recording an image may take many
18
19
20 minutes to hours. With coherent Raman techniques like SRS, a specific vibrational bond
21
22
23 can be probed using two lasers tuned to the bond's energy difference. This drives a
24
25
26
27
28 coherent resonance allowing video rate imaging to be achieved.¹³
29
30
31
32
33
34
35
36
37



5

1
2
3 **Figure 1.** Illustrative summary of different strategies for intracellular NP imaging.
4
5

6
7 Fluorescent dyes have been encapsulated in NPs to allow visualisation. Disadvantages
8
9
10 of this approach are that dye can leach out of the NPs and suffer from photobleaching.
11

12
13
14 In this work we directly label the polymer with a bioorthogonal Raman tag. Image
15
16
17 created with Biorender.com.
18
19

20
21
22 In contrast to infrared, Raman spectroscopy has a low background interference from
23
24
25 water making it ideally suited to study biological samples. Due to the absence of any
26
27
28 cellular vibrational peaks in the spectroscopic region between 1800 and 2800 cm^{-1} ,
29
30
31 known as the cell-silent region, small, bioorthogonal chemical tags (for example C-D,
32
33
34 C \equiv C and C \equiv N) which resonate in this region can be exploited to give imaging free of
35
36
37 cellular background.^{14–19} As such, poly(phenylene ethynylene) NPs, which have an
38
39
40 intrinsic alkyne, have been visualised in HeLa cells with spontaneous Raman imaging.²⁰
41
42
43
44
45
46 More recently, SRS has been used to image NP polymer dots bearing alkyne (2163 cm^{-1})
47
48
49

50
51 6
52
53
54
55
56
57
58
59
60

1
2
3
4 ¹), nitrile (2232 cm⁻¹) and carbon-deuterium (2293 cm⁻¹) bonds, which all produce peaks
5
6
7 in the cell silent region.²¹
8
9

10
11 In this work, we have explored two analogues of PLGA, with deuterium and alkyne
12
13 labels which are Raman active in the cell-silent region. These polymers were then
14
15 formulated into NPs and imaged firstly in cultured primary microglia and then in *ex vivo*
16
17 brain tissue by SRS microscopy. As opposed to imaging a fluorescent payload, our
18
19 approach allows direct imaging of the nanoparticle itself, and can be used to monitor the
20
21 cellular location of the NPs. SRS microscopy gives a signal enhancement over
22
23 spontaneous Raman imaging, and also a 1000 fold improvement in image acquisition
24
25 speed.²² We have therefore used SRS to image NP analogues of PLGA, a highly
26
27 relevant biocompatible and biodegradable polymer.
28
29
30
31
32
33
34
35
36
37
38
39
40
41
42

43 MATERIALS AND METHODS

44
45
46
47
48
49
50
51
52
53
54
55
56
57
58
59
60

7

1
2
3
4 **Synthesis of PLGA:** Under a nitrogen atmosphere D,L-lactide (8.0 g, 55 mmol) and
5
6
7 glycolide (2.8 g, 24 mmol) were added to a preheated round bottom flask containing
8
9
10
11 stannous octanoate (0.16 g, 0.40 mmol) and dodecanol (0.07 g, 0.40 mmol) at 130°C.
12
13
14 The reaction mixture was heated and stirred for a further hour until complete conversion
15
16
17 was reached. After the reaction was cooled to room temperature, it was dissolved in
18
19
20 dichloromethane (DCM) (5 mL) and precipitated in cold methanol (400 mL). The solvent
21
22
23 was decanted off, leaving a colorless solid which was dried *in vacuo* until constant
24
25
26
27 weight. ¹H NMR (500 MHz, Chloroform-d) δ 5.30 – 5.11 (9H, m, CH), 4.97 – 4.58 (7H,
28
29
30 m, CH₂), 1.64 – 1.49 (23H, m, CH₃); GPC *M_n* = 5700 g/mol, Đ = 1.11.
31
32
33
34
35

36 **Synthesis of PLGA-D:** D,L-Lactic acid (0.10 g, 0.94 mmol; 85% in water), L-lactic acid-d₃
37
38
39 (0.10 g, 0.91 mmol; 85% in water) and glycolic acid (0.06 g, 0.79 mmol) were
40
41
42 dehydrated at 150°C for 8 h in a flask fitted with an air condenser containing molecular
43
44
45
46 sieves to form oligomers. Tin chloride (0.5 wt%) and *para*-toluene sulfonic acid (0.5
47
48
49
50
51
52
53
54
55
56
57
58
59
60

1
2
3 wt%) were then added to the oligomers followed by heating to 180°C for a further 8 h.

4
5
6 The crude polymer was dissolved in DCM (2 mL) and precipitated into a 50:50 mixture

7
8 of ice-cold hexane/ether (100 mL) to yield a colorless solid which was dried *in vacuo*

9
10
11 until constant weight. ¹H NMR (400 MHz, Chloroform-d) δ 5.30-5.13 (1H, m, CH), 4.93-

12
13
14 4.56 (2H, m, CH₂), 1.64-1.51 (3H, m, CH₃). GPC *M*_n = 4553 g/mol, Đ = 1.84.

15
16
17
18
19
20
21 **Synthesis of PLGA-alkyne:** In a glovebox, PLGA (2.00 g, 0.56 mmol), propargyl-DOX

22
23 (0.38 g, 2.78 mmol, see Scheme S2), and SnOct₂ (0.23 g, 0.56 mmol) were dissolved in

24
25
26 toluene (4 mL) and charged to a Schlenk flask. The flask was removed from the

27
28
29 glovebox and heated at 110°C for 24 h. After the reaction was cooled to room

30
31
32
33 temperature, the reaction mixture was diluted further by the addition of DCM (5 mL) and

34
35
36 the mixture was precipitated in cold methanol (400 mL). The solvent was decanted off

37
38
39 leaving a colourless solid which was dried *in vacuo* until constant weight. ¹H NMR (500

1
2
3
4 MHz, Chloroform-d) δ 5.43 – 5.11 (m, 9H), 4.97 – 4.58 (m, 7H), 2.99 – 2.77 (m, 2H),
5
6
7 2.14 – 2.03 (br s, 1H), 1.64 – 1.49 (m, 23H). GPC M_n = 5900 g/mol, D = 1.88.
8
9

10
11 **Nanoparticle synthesis and characterisation:** A solution of PLGA-D/PLGA-alkyne (10-20
12
13
14 mg) in DCM (1 mL) was added to an aqueous solution of 1% polyvinyl alcohol (MW 31
15
16
17 000 – 50 000 Da, 98-99% hydrolysed) and 0.2% sodium dodecyl sulphate (10 mL). The
18
19
20
21
22 two phases were emulsified using a probe tip sonicator (Soniprep 150, MSE) for 2
23
24
25
26 minutes. The resulting emulsion was stirred at room temperature overnight to allow
27
28
29 evaporation of the DCM. The nanoparticles were collected by centrifugation at 8000 rpm
30
31
32 for 10 minutes, and washed once with deionised water. Nanoparticle tracking analysis
33
34
35
36 measurements were carried out in triplicate in 1 × PBS on a NanoSight LM10 (Malvern
37
38
39 Panalytical) for 60 seconds with the temperature measured for each individual run. The
40
41
42
43 samples were diluted until in the range of $1-8 \times 10^8$ particles mL⁻¹ for more accurate
44
45
46
47
48
49

50
51 10
52
53
54
55
56
57
58
59
60

1
2
3
4 measurements. Dynamic light scattering (DLS) was carried out on a Zetasizer Nano ZS
5
6
7 (Malvern Panalytical) in water at 25°C.
8
9

10
11 **Spontaneous Raman:** Spontaneous Raman spectra were acquired on a confocal

12
13
14 Raman spectrometer (inVia Raman microscope, Renishaw). A 297 mW (206 mW after
15
16
17 objective) 785 nm diode laser, or a 200 mW 532 nm laser excitation source was used to
18
19
20
21 excite the sample through a 20× or 50× objective. All spectra were background
22
23
24
25 subtracted using the background correction algorithm available on the Wire 4.4
26
27
28
29 software.
30
31
32

33 **SRS setup:** Images were acquired using a custom-built multi-modal microscope. A picoEmerald
34
35 (APE, Berlin, Germany) laser gave a tuneable pump laser (720-990 nm, 7 ps, 80 MHz repetition
36
37 rate) and a spatially and temporally overlapped Stokes laser (1064 nm, 5-6 ps, 80 MHz repetition
38
39 rate). Back scattered RFP two-photon fluorescence signals were filtered using the following
40
41 series of filters: FF552-Di02, FF440/520-Di01 (Semrock) and HQ610/75m (Chroma). For SRS
42
43
44 measurements, the Stokes beam was modulated with a 20 MHz EoM. Forward scattered light
45
46
47 was collected by a 20× Olympus XLUMPLFLN Objective, 1.00 NA lens and filtered
48
49
50

51 11
52
53
54
55
56
57
58
59
60

1
2
3 using ET890/220m filter (Chroma). A telescope focused the light onto an APE silicon
4
5 photodiode connected to an APE lock-in amplifier which was fed into the analogue unit of the
6
7 microscope.
8
9

10
11 The pump laser was tuned to 810.5 nm (2930 cm^{-1} , protein), 816 nm (2850 cm^{-1} , lipid),
12
13 867.5 nm (2128 cm^{-1} , $\text{C}\equiv\text{C}$) and 858.3 nm (2252 cm^{-1} , C-D), and laser powers after the
14
15 objective were measured up to 40-70 mW for the pump laser, and up to 70 mw for the
16
17 Stokes laser. All images were recorded at 512×512 or 1024×1024 pixels with a pixel
18
19 dwell time between 2 and 20 μs by FV10-ASW software (Olympus).
20
21
22
23
24
25
26
27
28
29

30 **General procedures for cell culture:** Microglia cultures were prepared from neonatal
31
32 Sprague-Dawley rats. Mixed glia cultures were isolated from postnatal day 1-2 rat pups,
33
34 and after 10 days microglia were isolated by shaking the culture flasks and relying on
35
36 differential adhesion of oligodendrocyte precursor cells, microglia and astrocytes.²³
37
38
39
40
41
42
43

44 Microglia were cultured in Dulbecco's Modified Eagle Media (Gibco) + 10% fetal bovine
45
46 serum + 1% penicillin streptomycin, and were incubated at 37°C in a humidified
47
48
49

50
51 12
52
53
54
55
56
57
58
59
60

1
2
3 atmosphere with 7.5% CO₂ and media changes every 2-3 days. To improve cell
4
5
6
7 adherence, all culture dishes were coated in poly-D-lysine before plating the cells by
8
9
10 covering dishes in a 1 µg/mL aqueous solution and incubating at 37°C for one hour,
11
12
13
14 before removing the solution and washing once with sterile water. Cell fixation was
15
16
17 achieved by covering the cells with a solution of 4% formaldehyde (2 mL) for 10 minutes
18
19
20
21 at room temperature before washing three times with 1 × PBS (3 × 2 mL).
22
23
24

25 **SRS microglia experiments:** Microglia were plated at 3×10^5 cells per well in FluoroDish
26
27
28 Cell Culture Dishes (World Precision Instruments) and left overnight to adhere to the
29
30
31 dish. NPs (alkyne or deuterium) were then added at 2×10^9 particles mL⁻¹ followed by a
32
33
34
35
36 24 hour incubation. The media was then removed and the cells were washed twice with
37
38
39 1 × PBS (2 × 2 mL) before fixation and imaging with the SRS set-up described above.
40
41
42

43 **Slice culture experiments:** Brains were isolated from P5 C57BL6/N mice pups in cold
44
45 Hibernate-A medium (Thermo Fisher A12475-01) on ice and cut into 300 µm cortical slices
46
47 using a vibratome (Leica). The slices were then transferred to Millipore milli cell-CM
48
49

50
51 13
52
53
54
55
56
57
58
59
60

1
2
3 organotypic inserts (30 mm, hydrophilic PTFE, 0.4 μm , Merck-Millipore, PICM0RG50) in slice
4
5 media (50% MEM (Invitrogen, 32360-026) with 25% Earle's Balanced Salt Solution
6
7 (Invitrogen, 24010-043), 25% heat-inactivated horse serum (Invitrogen, 26050-088), 1%
8
9 glutamax supplement (Invitrogen, 35050-038), 1% penicillin–streptomycin, 0.5% Fungizone
10
11 (Invitrogen, 15290-018) and 6.5 mg/ml glucose (Sigma G8769)), and were maintained at 37 °C
12
13 and 7.5% CO₂ with media changes every two days. After 6 days in culture, alkyne NPs were
14
15 added at 2×10^8 and 2×10^9 particles mL⁻¹ for 24 hours. The slices were then washed twice with
16
17 $1 \times$ PBS (2×2 mL) before fixation. Slices were fixed with 4% formaldehyde (2 mL) for one
18
19 hour at room temperature before washing three times with $1 \times$ PBS (3×2 mL).
20
21
22
23
24

25 **Immunostaining of slices:** Fixed slices in a 6 well plate were incubated with blocking
26
27 solution (3% HIHS, 2% BSA, 0.5% Triton in PBS) (1 mL per well) for 2 h before adding
28
29 the primary antibodies. Rabbit polyclonal anti-IBA1 (1/500, Abcam, AB178846) and
30
31 mouse monoclonal anti-OLIG2 (1/500, Merck Millipore, MABN50) were diluted in
32
33 blocking solution and 500 μL was added to each well. The slices were then shaken at 4
34
35 °C for 1.5 days before washing three times for 1 h with blocking solution (3×2 mL). The
36
37 secondary antibodies, goat anti-rabbit 568 (1/1000, Life Technologies, A11011) and donkey anti-
38
39 mouse 488 (1/1000, Thermo Fisher Scientific, A21202) were diluted in blocking solution and
40
41
42
43
44
45
46
47
48
49

50
51 14
52
53
54
55
56
57
58
59
60

1
2
3 then incubated with the slices (500 μ L per well) with gentle agitation overnight, in the dark at 4
5
6
7 $^{\circ}$ C. The slices were then washed once for 10 minutes followed by three 1 h washes with
8
9
10 1 \times PBS (4 \times 2 mL) and finally imaged using the SRS set-up described above.

11
12
13
14 **Image processing:** All images were processed with the Fiji image processing package
15
16 (<https://imagej.net/Fiji>). False colour assignments and scale bars were added to images. Image
17
18 overlays and orthogonal views were also processed with Fiji.

21 22 RESULTS AND DISCUSSION

23
24
25
26 Deuterated PLGA (PLGA-D) was synthesised via a direct poly-condensation method
27
28
29 from lactic acid, lactic acid- d_3 and glycolic acid, which produced a polymer with a
30
31
32
33 molecular weight of 4.5 kDa and a dispersity of 1.84 (Scheme 1A).^{24,25} Since Raman is
34
35
36 an inherently weak effect, with only approximately 1 in every 10^8 molecules
37
38
39
40 experiencing Raman scattering,²⁶ a deuterium group was introduced into the monomer,
41
42
43
44 as opposed to substitution onto a pre-made polymer, to maximise the Raman signal of
45
46
47 the NPs.

48
49
50
51 15
52
53
54
55
56
57
58
59
60

1
2
3 To produce the alkyne analogue of PLGA (PLGA-alkyne), PLGA was first synthesised
4
5
6
7 by a ring opening copolymerisation of lactide and glycolide, using dodecanol as the
8
9
10 initiator and stannous octanoate as the catalyst.²⁷ Recent work has shown that 1,3-
11
12
13 dioxolan-4-ones (DOX) are a versatile and sustainable family of monomers utilised for
14
15
16
17 the synthesis of biodegradable polyesters by ring opening polymerisation.^{28,29} To
18
19
20
21 introduce the alkyne functionality, the telechelic properties of PLGA were exploited to
22
23
24 initiate the polymerisation of propargyl-DOX (see Scheme S.2 for propargyl-DOX
25
26
27
28 synthesis). Ring-opening polymerisation from the PLGA macroinitiator initially affords a
29
30
31 blocky PLGA-P(propargyl-DOX) copolymer. However, extended reaction times lead to
32
33
34
35 transesterification catalysed by stannous octanoate, scrambling the terpolymer structure
36
37
38
39 to afford a statistical distribution of the alkyne units throughout the PLGA chain (Scheme
40
41
42 1B). This gave rise to a polymer with comparable molecular weight and dispersity to the
43
44
45 deuterium analogue (5.9 kDa and 1.88 respectively). The incorporation of the alkyne
46
47
48
49
50
51
52
53
54
55
56
57
58
59
60

1
2
3 into the terpolymer was confirmed by a single cross peak in the diffusion-ordered
4
5
6
7 spectroscopy (DOSY) NMR (Figure S2).
8
9
10
11
12
13
14
15
16
17
18
19
20
21
22
23
24
25
26
27
28
29



30 **Scheme 1.** Synthesis of Raman active PLGA analogues. A) Synthesis of PLGA-D.
31
32 Reagents and conditions: a; 150°C, 8 h, b; SnCl₂, *p*-TSA, 180°C, 8 h. B) Synthesis of
33
34 PLGA-alkyne. Reagents and conditions: c; Sn(oct)₂, toluene, 110°C, 24 h.
35
36
37
38
39
40
41
42
43

44 The Raman labelled polymers, along with unlabelled PLGA, were then characterised
45
46
47 with spontaneous Raman spectroscopy (Figure 2). PLGA (black) was analysed as a
48
49

50
51 17
52
53
54
55
56
57
58
59
60

control to show that there are no peaks in the cell-silent region. In contrast, the PLGA-D (red) shows multiple broad peaks between 2000 and 2300 cm^{-1} , and the PLGA-alkyne (blue) shows a single, intense peak at 2128 cm^{-1} . Notably, the alkyne signal presents a much stronger peak in the cell silent region than the deuterium, which is consistent with previous studies.¹⁷

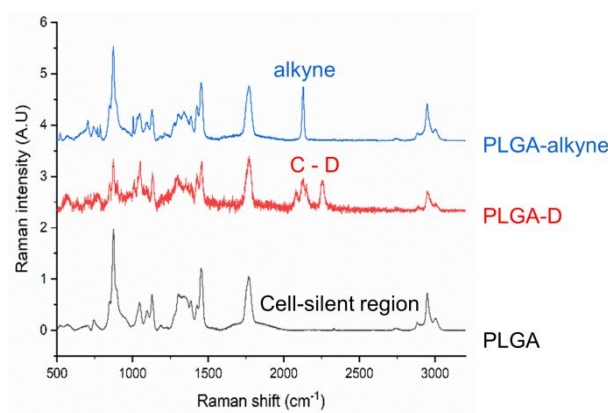


Figure 2. Analysis of polymers by Spontaneous Raman spectroscopy. Spontaneous Raman spectra of PLGA (black), PLGA-D (red) and PLGA-alkyne (blue), with the labelled analogues showing peaks in the cell silent region. Spectra are normalised to the carbonyl peak (C=O) at 1737 cm^{-1} and offset for clarity, $\lambda_{\text{ex}}=785 \text{ nm}$.

1
2
3
4
5
6
7 The PLGA analogues were then fabricated into NPs using the standard, and widely
8
9
10 used, emulsification-evaporation method (Figure 3A),³⁰ which can be easily modified to
11
12
13 encapsulate both hydrophobic and hydrophilic drugs. The NPs were analysed by
14
15
16
17 nanoparticle tracking analysis (NTA), a technique which uses an optical microscope
18
19
20
21 equipped with a laser to visualise particles according to the light they scatter.^{31,32}
22
23
24 Individual particles were then tracked and their Brownian motion measured, which gives
25
26
27
28 both particle size and particle concentration data (Figure 3B). This showed that the
29
30
31 mean size of the PLGA-D and PLGA-alkyne particles are 87 and 81 nm respectively.
32
33
34
35 Visualisation of the particles by the NTA shows that they are uniform and well separated
36
37
38 (Figure 3C). Due to the tendency of the PLGA-D NPs to aggregate over time (Figure
39
40
41
42 S4), the NPs were freshly prepared before every biological experiment.
43
44
45
46
47
48
49
50

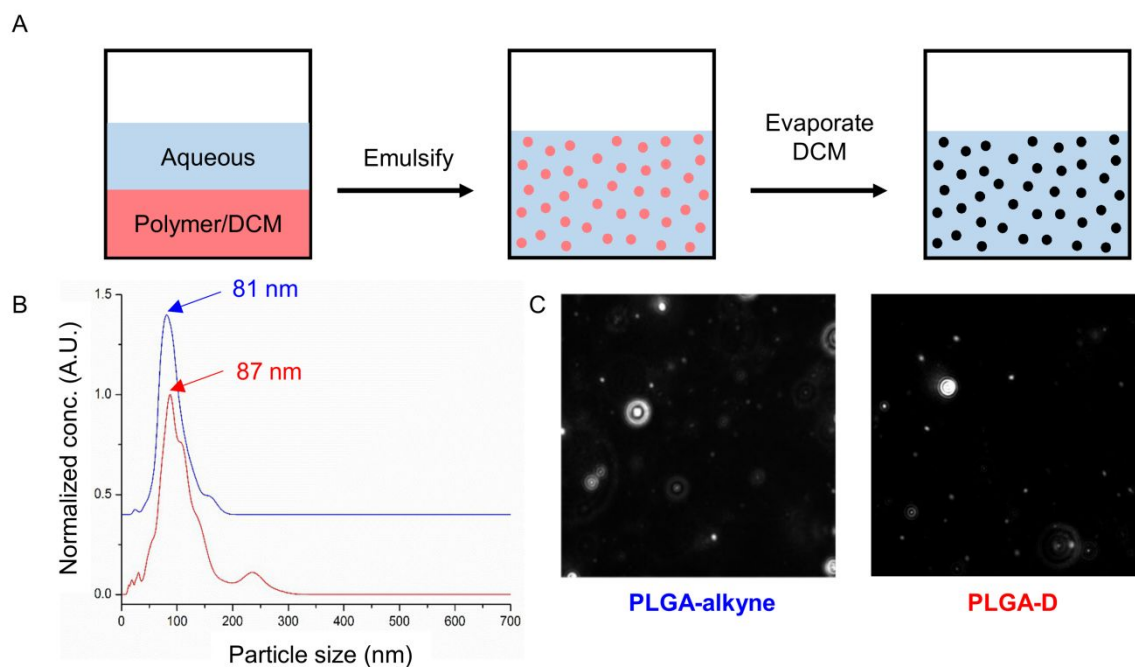


Figure 3. The synthesis and characterization of polymer NPs. A) A general representation of the emulsification- evaporation process. B) Particle size distribution acquired from the NTA of PLGA-alkyne (blue) and PLGA-D (red). Spectra are normalised between 0 and 1 and offset for clarity. C) A visual representation of the NPs detected by the NTA camera, which is proportional to the amount of light scattered by the particles.

1
2
3
4 Next, we treated primary rat microglia with our two Raman active NPs. We chose
5
6
7 microglia as 'proof of principle' cells as they are phagocytes in the brain, and therefore
8
9
10 likely to internalise the NPs.³³ NPs can cross the blood-brain barrier, and so have great
11
12
13 potential for delivery of cargo to the brain.^{34,35} The microglia used were primary cultures
14
15
16 isolated from rat brains to retain more biologically relevant *in vivo* characteristics as
17
18
19 opposed to using cell lines.
20
21
22
23

24 To test whether NPs were toxic to microglia, we used a luminescence cell viability
25
26
27 assay which quantifies the amount of ATP, indicative of live cells. This assay found that
28
29
30 PLGA, PLGA-D and PLGA-alkyne NPs were all non-toxic to microglia at all
31
32
33 concentrations tested (1, 2 and 4×10^9 particles mL⁻¹) (Figure S5).
34
35
36
37

38 Microglia were then incubated with PLGA-D or PLGA-alkyne NPs for 24 hours before
39
40
41 imaging with SRS microscopy (Figure 4). Tuning the energy difference between the
42
43
44 pump and Stokes beams of the SRS microscope to 2939 cm⁻¹ excites CH₃ vibrations
45
46
47 only, showing the protein content of the cells. Similarly, tuning to 2856 cm⁻¹ excites CH₂
48
49
50
51 21
52
53
54
55
56
57
58
59
60

1
2
3 vibrations, which is indicative of the cellular lipid content. Due to the bioorthogonal
4
5
6
7 deuterium and alkyne chemical labels on our NPs, tuning to 2253 cm^{-1} (C-D) and 2128
8
9
10 cm^{-1} (C≡C) respectively allowed visualisation of the cellular location of the NPs, which
11
12
13
14 were shown to be distributed throughout the cytoplasm and absent from the nuclei. Z-
15
16
17 stack analysis of the cells also confirmed that the NPs had been internalised (Figure
18
19
20
21 S6).

22
23
24 Time dependent analysis of PLGA-alkyne NP internalisation into microglia was also
25
26
27 carried out over 24 hours. The alkyne intensity of individual cells at 0, 12 and 24 hours
28
29
30
31 were quantified, and this showed that the alkyne intensity, and therefore the intensity of
32
33
34
35 NPs, increased over time (Figure S7).

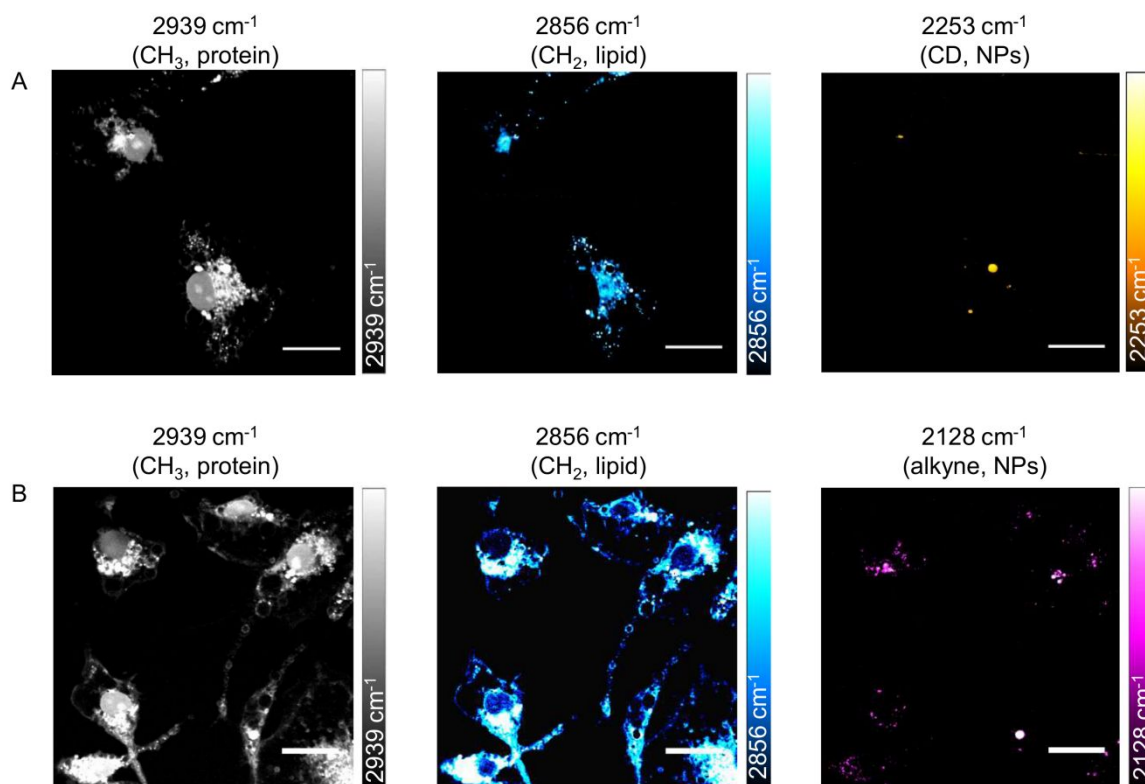


Figure 4. SRS imaging of NPs in microglia. Microglia were incubated with PLGA-D NPs (A) or PLGA-alkyne NPs (B) at 2×10^9 particles mL⁻¹ for 24 hours before fixing and imaging with SRS microscopy. Scale bars 20 μm.

As predicted by inspection of the spontaneous Raman spectra in Figure 2, the PLGA-alkyne NPs gave a stronger intracellular signal compared to PLGA-D. For this reason,

23

1
2
3 we chose to carry out further studies with the PLGA-alkyne NPs only. Using a multi-
4
5
6
7 modal approach to imaging, NPs encapsulating rhodamine were visualised using SRS
8
9
10 (2128 cm^{-1} , NP) and two photon fluorescence (866 nm and 1064 nm, rhodamine) and
11
12
13
14 the signals were shown to co-localise after 24 h incubation demonstrating that this
15
16
17 model payload could be delivered to microglia using these novel PLGA-alkyne NPs
18
19
20
21 (Figure S8).
22
23

24 We then went on to investigate the uptake of the alkyne NPs in *ex vivo* mouse brain
25
26
27 slices. These slices were freshly harvested from mice pups and cultured, bridging the
28
29
30 gap between *in vitro* cell culture and *in vivo* experiments in rodents.³⁶ The slices were
31
32
33
34 incubated with alkyne NPs at 2×10^8 and 2×10^9 particles mL^{-1} for 24 hours before
35
36
37
38 washing, fixing and imaging with SRS microscopy. SRS imaging at 2128 cm^{-1} showed
39
40
41
42 that there are alkyne NPs distributed throughout the tissue.
43
44

45 To determine if the NPs were inside cells in the brain tissue, and what type of cells
46
47
48 these were, a multimodal imaging technique of both immunofluorescence and Raman
49
50
51 24
52
53
54
55
56
57
58
59
60

1
2
3
4 imaging was employed. Immunofluorescence uses primary antibodies which bind to
5
6
7 markers specific to a certain cell type, and then secondary fluorescent antibodies so
8
9
10 that the cells can be visualised by fluorescence microscopy. We used a primary
11
12
13 antibody to the protein IBA1, which is found specifically on microglia, and also an
14
15
16 antibody to OLIG2 to label oligodendroglia, which are glia that would not be expected to
17
18
19 phagocytose NPs. Figure 5A shows the immunostained tissue with microglia in red,
20
21
22 oligodendrocytes in green and NPs in magenta. This clearly shows the association of
23
24
25 the NPs with microglia at both concentrations tested. Z-stack analysis of the tissue also
26
27
28 allowed depth analysis of the NP location, with Figure 5B showing a Z-stack with
29
30
31 orthogonal views of the tissue. It is clear from this image that the NPs have been
32
33
34 internalised by microglia, although there are many other microglia that do not contain
35
36
37 NPs, suggesting that uptake is not as homogeneous as it was with the *in vitro* microglia
38
39
40
41
42
43
44
45 cultures.

46
47
48
49
50
51 25
52
53
54
55
56
57
58
59
60

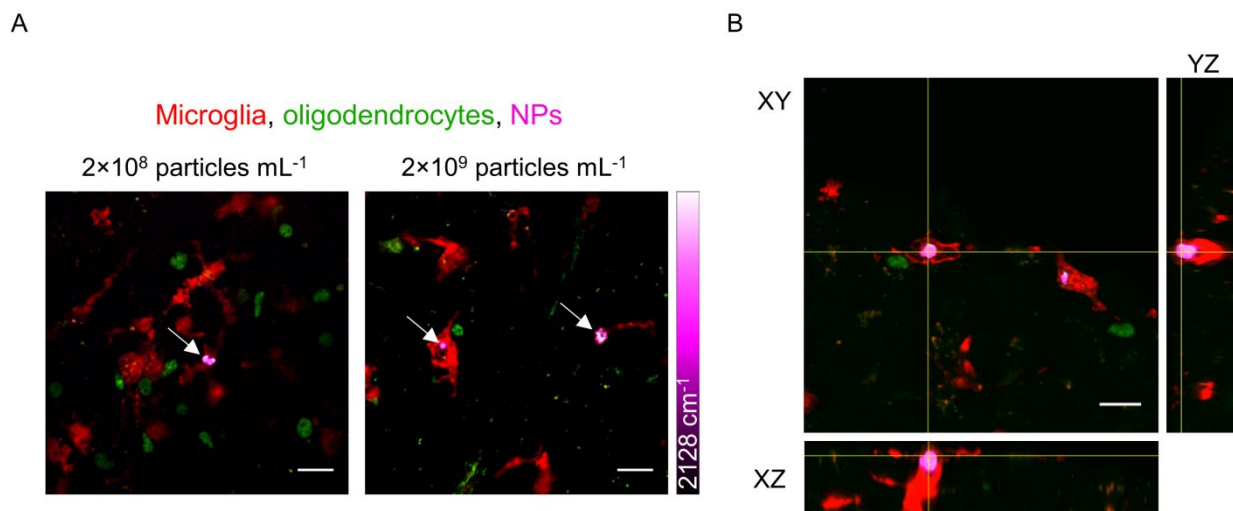


Figure 5. Imaging alkyne NPs in *ex vivo* brain slices. A) Alkyne NPs were added to *ex vivo* mouse cortical brain slices at 2×10^8 and 2×10^9 particles mL^{-1} for 24 hours before washing, fixing and immunostaining. Microglia are shown in red (using antibodies against IBA1), oligodendrocytes in green (using antibodies against OLIG2) and NPs in magenta. Scale bars 20 μm . B) Orthogonal views of Z-stack images show that the NPs are inside microglia. Scale bar 20 μm .

1
2
3
4 These experiments have highlighted the clear capability of SRS to image our novel
5
6
7 PLGA-alkyne NPs in *ex vivo* brain tissue, and show that they are preferentially taken up
8
9
10 by microglia over oligodendroglia, which give them potential for targeted drug delivery.
11
12
13
14
15
16

17 CONCLUSIONS

18
19
20
21 Raman imaging, and specifically SRS microscopy, have the potential to give non-
22
23
24 invasive information about the location and state of polymeric nanocarriers in biological
25
26
27
28 environments. We have developed two Raman active analogues of PLGA, one of the
29
30
31 most commonly used biodegradable polymers for drug delivery research with a long
32
33
34
35 history and proven safety record,³⁷ and have used the location of these deuterium and
36
37
38 alkyne tags in the cell-silent region to enhance contrast of the NPs in a biological
39
40
41
42 environment. As neither deuterium nor alkyne bonds are present in biological samples,
43
44
45 the signal is certain to derive from the NPs. These NPs have been shown to be non-
46
47
48
49 toxic to living cells and SRS imaging has shown that both PLGA-D and PLGA-alkyne
50
51 27
52
53
54
55
56
57
58
59
60

1
2
3 NPs are internalized in primary rat microglia, and additionally the PLGA-alkyne NPs
4
5
6
7 were imaged in mouse cortical *ex vivo* brain slices. We believe that the strong Raman
8
9
10 signal obtained from the alkyne NPs gives them an especially wide ranging imaging
11
12
13 potential in many biological applications, including live animal studies which will be a
14
15
16
17 focus of our future work.
18
19

20 ASSOCIATED CONTENT

21
22
23
24
25 **Supporting Information.** Supporting information is available which shows the synthetic
26
27
28 route to propargyl DOX, selected NMR spectra including DOSY NMR, aqueous stability
29
30
31 of the NPs, time dependent analysis of PLGA-alkyne NPs in microglia, results from the
32
33
34 cell viability assay, Z-stacks of alkyne NPs inside microglia and images showing
35
36
37 encapsulation of rhodamine inside PLGA-alkyne NPs.
38
39
40

41 AUTHOR INFORMATION

42 43 44 45 46 47 48 **Corresponding Author**

49
50
51 28
52
53
54
55
56
57
58
59
60

1
2
3
4 *Alison N. Hulme, Alison.Hulme@ed.ac.uk
5
6
7

8 **Present Addresses**

9

10
11 †Michael P. Shaver, School of Materials and Henry Royce Institute, University of
12
13
14
15 Manchester
16
17
18

19 **Author Contributions**

20

21
22
23 ANH, AW, VGB, MPS, SC and SVH designed the experiments. SVH, SC, ML and LZ
24
25
26 carried out the experiments. SVH, ANH and MPS wrote the manuscript. SVH, SC, ML,
27
28
29
30 LZ, MPS, VGB, AW and ANH read and edited the manuscript.
31
32
33

34 **Funding Sources**

35
36
37
38

39 This work was funded by the BBSRC [EASTBIO studentship to SVH; grant ref.
40
41
42 BB/M010996/1] the EPSRC [grant to MPS, grant ref. EP/P026095/1], Cancer Research
43
44
45 UK [grant ref: C157/A25140 and C157/A15703], and the MS Society UK.
46
47
48
49

50
51 29
52
53
54
55
56
57
58
59
60

1
2
3
4
5
6
7
8
9
10
11
12
13
14
15
16
17
18
19
20
21
22
23
24
25
26
27
28
29
30
31
32
33
34
35
36
37
38
39
40
41
42
43
44
45
46
47
48
49
50
51
52
53
54
55
56
57
58
59
60

ACKNOWLEDGMENTS

We thank Dr Colin Campbell for use of the spontaneous Raman microscope [UK Regenerative Medicine Platform Niche Hub, MRC grant ref. MR/K026666/1]. We thank Dr Marie Bechler, Dr Matthew Swire and Monica Kim for the gift of microglia.

ABBREVIATIONS

DCM, dichloromethane; NPs, nanoparticles; PBS, phosphate buffered saline; PLGA, Poly(lactic acid-co-glycolic acid); SRS, stimulated Raman scattering.

REFERENCES

- (1) Tran, S.; Degiovanni, P.-J.; Piel, B.; Rai, P. Cancer Nanomedicine : A Review of Recent Success in Drug Delivery. *Clin. Transl. Med.* **2017**, *6*(44), 1–21.
<https://doi.org/10.1186/s40169-017-0175-0>.

- (2) Wicki, A.; Witzigmann, D.; Balasubramanian, V.; Huwyler, J. Nanomedicine in

- 1
2
3
4 Cancer Therapy: Challenges, Opportunities, and Clinical Applications. *J. Control.*
5
6
7 *Release* **2015**, *200*, 138–157. <https://doi.org/10.1016/j.jconrel.2014.12.030>.
8
9
10
11 (3) Rittchen, S.; Boyd, A.; Burns, A.; Park, J.; Fahmy, T. M.; Metcalfe, S.; Williams, A.
12
13
14 Myelin Repair in Vivo Is Increased by Targeting Oligodendrocyte Precursor Cells
15
16
17
18 with Nanoparticles Encapsulating Leukaemia Inhibitory Factor (LIF). *Biomaterials*
19
20
21
22 **2015**, *56*, 78–85. <https://doi.org/10.1016/j.biomaterials.2015.03.044>.
23
24
25
26 (4) Dong, X. Current Strategies for Brain Drug Delivery. *Theranostics* **2018**, *8* (6),
27
28
29 1481–1493. <https://doi.org/10.7150/thno.21254>.
30
31
32
33
34 (5) Qi, F.; Wu, J.; Li, H.; Ma, G. Recent Research and Development of PLGA/PLA
35
36
37
38 Microspheres/Nanoparticles: A Review in Scientific and Industrial Aspects. *Front.*
39
40
41
42 *Chem. Sci. Eng.* **2018**, 1–14. <https://doi.org/10.1007/s11705-018-1729-4>.
43
44
45
46 (6) Jonderian, A.; Maalouf, R. Formulation and in Vitro Interaction of Rhodamine-B
47
48
49
50 Loaded PLGA Nanoparticles with Cardiac Myocytes. *Front. Pharmacol.* **2016**, *7*

31

- (DEC), 1–7. <https://doi.org/10.3389/fphar.2016.00458>.
- (7) Vanden-Hehir, S.; Tipping, W. J.; Lee, M.; Brunton, V. G.; Williams, A.; Hulme, A. N. Raman Imaging of Nanocarriers for Drug Delivery. *Nanomaterials* **2019**, *9* (341), 1–19. <https://doi.org/10.3390/nano9030341>.
- (8) Kalluru, R.; Fenaroli, F.; Westmoreland, D.; Ulanova, L.; Maleki, A.; Roos, N.; Paulsen Madsen, M.; Koster, G.; Egge-Jacobsen, W.; Wilson, S.; Roberg-Larsen, H.; Khuller, G. K.; Singh, A.; Nystrom, B.; Griffiths, G. Poly(Lactide-Co-Glycolide)-Rifampicin Nanoparticles Efficiently Clear Mycobacterium Bovis BCG Infection in Macrophages and Remain Membrane-Bound in Phago-Lysosomes. *J. Cell Sci.* **2013**, *126* (14), 3043–3054. <https://doi.org/10.1242/jcs.121814>.
- (9) Gentile, P.; Chiono, V.; Carmagnola, I.; Hatton, P. V. An Overview of Poly(Lactic-Co-Glycolic) Acid (PLGA)-Based Biomaterials for Bone Tissue Engineering. *Int. J. Mol. Sci.* **2014**, *15* (3), 3640–3659. <https://doi.org/10.3390/ijms15033640>.

- 1
2
3
4 (10) Vicente, N. B.; Diaz Zamboni, J. E.; Adur, J. F.; Paravani, E. V.; Casco, V. H.
5
6
7 Photobleaching Correction in Fluorescence Microscopy Images. *J. Phys. Conf.*
8
9
10 *Ser.* **2007**, *90* (1). <https://doi.org/10.1088/1742-6596/90/1/012068>.
11
12
13
14 (11) Tipping, W. J.; Lee, M.; Serrels, A.; Brunton, V. G.; Hulme, A. N. Stimulated
15
16
17 Raman Scattering Microscopy: An Emerging Tool for Drug Discovery. *Chem. Soc.*
18
19
20
21 *Rev.* **2016**, *45* (8), 2075–2089. <https://doi.org/10.1039/C5CS00693G>.
22
23
24
25
26 (12) Krafft, C.; Schie, I. W.; Meyer, T.; Schmitt, M.; Popp, J. Developments in
27
28
29 Spontaneous and Coherent Raman Scattering Microscopic Imaging for
30
31
32
33 Biomedical Applications. *Chem. Soc. Rev.* **2016**, *45* (7), 1819–1849.
34
35
36 <https://doi.org/10.1039/c5cs00564g>.
37
38
39
40
41 (13) Yakovlev, V. V.; Petrov, G. I.; Zhang, H. F.; Noojin, G. D.; Denton, M. L.; Thomas,
42
43
44 R. J.; Scully, M. O. Stimulated Raman Scattering: Old Physics, New Applications.
45
46
47 *J. Mod. Opt.* **2009**, *56* (18–19), 1970–1973.
48
49

1
2
3
4 <https://doi.org/10.1080/09500340903082671>.

- 5
6
7
8 (14) Li, Y.; Wang, Z.; Mu, X.; Ma, A.; Guo, S. Raman Tags: Novel Optical Probes for
9
10 Intracellular Sensing and Imaging. *Biotechnol. Adv.* **2017**, *35* (2), 168–177.

11
12
13
14
15 <https://doi.org/10.1016/j.biotechadv.2016.12.004>.

- 16
17
18
19 (15) Wei, L.; Hu, F.; Shen, Y.; Chen, Z.; Yu, Y.; Lin, C. C.; Wang, M. C.; Min, W. Live-
20
21 Cell Imaging of Alkyne-Tagged Small Biomolecules by Stimulated Raman
22
23 Scattering. *Nat. Methods* **2014**, *11* (4), 410–412.

24
25
26
27
28
29
30 <https://doi.org/10.1038/nmeth.2878>.

- 31
32
33
34 (16) Hong, S.; Chen, T.; Zhu, Y.; Li, A.; Huang, Y.; Chen, X. Live-Cell Stimulated
35
36 Raman Scattering Imaging of Alkyne-Tagged Biomolecules. *Angew. Chem. - Int.*
37
38 *Ed.* **2014**, *53* (23), 5827–5831. <https://doi.org/10.1002/anie.201400328>.

- 39
40
41
42
43
44
45 (17) Yamakoshi, H.; Dodo, K.; Palonpon, A.; Ando, J.; Fujita, K.; Kawata, S.; Sodeoka,
46
47
48 M. Alkyne-Tag Raman Imaging for Visualization of Mobile Small Molecules in Live

49
50
51 34

1
2
3
4 Cells. *J. Am. Chem. Soc.* **2012**, *134* (51), 20681–20689.

5
6
7 <https://doi.org/10.1021/ja308529n>.

8
9
10
11 (18) Tipping, W. J.; Lee, M.; Serrels, A.; Brunton, V. G.; Hulme, A. N. Imaging Drug

12
13
14 Uptake by Bioorthogonal Stimulated Raman Scattering Microscopy. *Chem. Sci.*

15
16
17
18 **2017**, *8* (8), 5606–5615. <https://doi.org/10.1039/c7sc01837a>.

19
20
21
22 (19) Zhao, Z.; Shen, Y.; Hu, F.; Min, W. Applications of Vibrational Tags in Biological

23
24
25
26 Imaging by Raman Microscopy. *Analyst*. **2017**, pp 4018–4029.

27
28
29
30 <https://doi.org/10.1039/c7an01001j>.

31
32
33 (20) Li, S.; Chen, T.; Wang, Y.; Liu, L.; Lv, F.; Li, Z.; Huang, Y.; Schanze, K. S.; Wang,

34
35
36
37 S. Conjugated Polymer with Intrinsic Alkyne Units for Synergistically Enhanced

38
39
40
41 Raman Imaging in Living Cells. *Angew. Chem. - Int. Ed.* **2017**, *56* (43), 13455–

42
43
44
45 13458. <https://doi.org/10.1002/anie.201707042>.

46
47
48 (21) Hu, F.; Brucks, S. D.; Lambert, T. H.; Campos, L. M.; Min, W. Stimulated Raman

49
50
51 35

- 1
2
3
4 Scattering of Polymer Nanoparticles for Multiplexed Live-Cell Imaging. *Chem.*
5
6
7 *Commun.* **2017**, *53* (46), 6187–6190. <https://doi.org/10.1039/c7cc01860f>.
8
9
10
11 (22) Min, W.; Freudiger, C. W.; Lu, S.; Xie, X. S. Coherent Nonlinear Optical Imaging:
12
13
14 Beyond Fluorescence Microscopy. *Annu. Rev. Phys. Chem.* **2011**, *62* (1), 507–
15
16
17
18 530. <https://doi.org/10.1146/annurev.physchem.012809.103512>.
19
20
21
22 (23) McCarthy, K. D.; de Vellis, J. Preparation of Separate Astroglial and
23
24
25
26 Oligodendroglial Cell Cultures from Rat Cerebral Tissue. *J. Cell Biol.* **1980**, *85*
27
28
29 (June), 890–902.
30
31
32
33 (24) Moon, S. II; Lee, C. W.; Miyamoto, M.; Kimura, Y. Melt Polycondensation of L-
34
35
36
37 Lactic Acid with Sn(II) Catalysts Activated by Various Proton Acids: A Direct
38
39
40
41 Manufacturing Route to High Molecular Weight Poly(L-Lactic Acid). *J. Polym. Sci.*
42
43
44 *Part A Polym. Chem.* **2000**, *38* (9), 1673–1679.
45
46
47
48 [https://doi.org/10.1002/\(SICI\)1099-0518\(20000501\)38:9<1673::AID-](https://doi.org/10.1002/(SICI)1099-0518(20000501)38:9<1673::AID-)
49

- 1
2
3 POLA33>3.0.CO;2-T.
4
5
6
7
8 (25) Gao, Q.; Lan, P.; Shao, H.; Hu, X. Direct Synthesis with Melt Polycondensation
9
10 and Microstructure Analysis of Poly(L-Lactic Acid-Co-Glycolic Acid). *Polym. J.*
11
12 **2002**, *34* (11), 786–793. <https://doi.org/10.1295/polymj.34.786>.
13
14
15
16
17
18
19 (26) Ember, K. J. I.; Hovee, M. A.; McAughtrie, S. L.; Bergholt, M. S.; Dwyer, B. J.;
20
21
22 Stevens, M. M.; Faulds, K.; Forbes, S. J.; Campbell, C. J. Raman Spectroscopy
23
24 and Regenerative Medicine: A Review. *npj Regen. Med.* **2017**, *2* (1), 12.
25
26
27 <https://doi.org/10.1038/s41536-017-0014-3>.
28
29
30
31
32
33
34 (27) Erbetta, C. D. C.; Alves, R. J.; Resende, J. M.; Freitas, R. F. de S.; Geraldo de
35
36
37 Sousa, R. Synthesis and Characterization of Poly(D,L-Lactide-Co-Glycolide)
38
39
40
41 Copolymer. *J. Biomater. Nanobiotechnol.* **2012**, *3*, 208–225.
42
43
44 <https://doi.org/http://dx.doi.org/10.4236/jbnb.2012.32027>.
45
46
47
48 (28) Cairns, S. A.; Schultheiss, A.; Shaver, M. P. A Broad Scope of Aliphatic
49
50
51 37
52
53
54
55
56
57
58
59
60

1
2
3 Polyesters Prepared by Elimination of Small Molecules from Sustainable 1,3-

4
5
6
7 Dioxolan-4-Ones. *Polym. Chem.* **2017**, *8* (19), 2990–2996.

8
9
10 <https://doi.org/10.1039/c7py00254h>.

11
12
13
14
15 (29) Xu, Y.; Perry, M. R.; Cairns, S. A.; Shaver, M. P. Understanding the Ring-Opening

16
17
18 Polymerisation of Dioxolanones. *Polym. Chem.* **2019**.

19
20
21 <https://doi.org/10.1039/c8py01695j>.

22
23
24
25
26 (30) Feczko, T.; Tóth, J.; Dósa, G.; Gyenis, J. Influence of Process Conditions on the

27
28
29 Mean Size of PLGA Nanoparticles. *Chem. Eng. Process. Process Intensif.* **2011**,

30
31
32
33 *50* (8), 846–853. <https://doi.org/10.1016/j.cep.2011.05.006>.

34
35
36
37 (31) Filipe, V.; Hawe, A.; Jiskoot, W. Critical Evaluation of Nanoparticle Tracking

38
39
40 Analysis (NTA) by NanoSight for the Measurement of Nanoparticles and Protein

41
42
43
44
45
46
47
48
49
50
51
52
53
54
55
56
57
58
59
60
Aggregates. *Pharm. Res.* **2010**, *27* (5), 796–810. [https://doi.org/10.1007/s11095-](https://doi.org/10.1007/s11095-010-0073-2)

010-0073-2.

- 1
2
3
4 (32) Gross, J.; Sayle, S.; Karow, A. R.; Bakowsky, U.; Garidel, P. Nanoparticle
5
6
7 Tracking Analysis of Particle Size and Concentration Detection in Suspensions of
8
9
10 Polymer and Protein Samples: Influence of Experimental and Data Evaluation
11
12
13 Parameters. *Eur. J. Pharm. Biopharm.* **2016**, *104*, 30–41.
14
15
16
17 <https://doi.org/10.1016/j.ejpb.2016.04.013>.
18
19
20
21 (33) Vilhardt, F. Microglia: Phagocyte and Glia Cell. *Int. J. Biochem. Cell Biol.* **2005**, *37*
22
23
24 (1), 17–21. <https://doi.org/10.1016/j.biocel.2004.06.010>.
25
26
27
28
29 (34) Neha, B.; Ganesh, B.; Preeti, K. Drug Delivery to The Brain Using Polymeric
30
31
32 Nanoparticles: A Review. *Int. J. Pharm. Life Sci.* **2013**, *2*(3), 107–132.
33
34
35
36 <https://doi.org/10.3329/ijpls.v2i3.15457>.
37
38
39
40 (35) Masserini, M. Nanoparticles for Brain Drug Delivery. *ISRN Biochem.* **2013**, *2013*,
41
42
43
44 238428. <https://doi.org/10.1155/2013/238428>.
45
46
47
48 (36) Zhang, H.; Jarjour, A. A.; Boyd, A.; Williams, A. Central Nervous System
49
50
51 39
52
53
54
55
56
57
58
59
60

1
2
3 Remyelination in Culture — A Tool for Multiple Sclerosis Research. *Exp. Neurol.*

4
5
6
7 2011, 230 (1), 138–148. <https://doi.org/10.1016/j.expneurol.2011.04.009>.

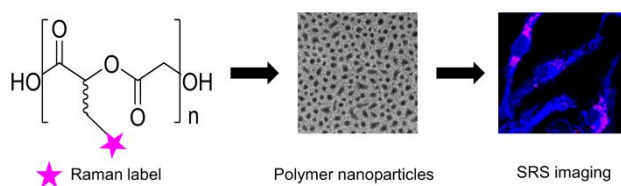
8
9
10
11 (37) Pappalardo, D.; Mathisen, T.; Finne-Wistrand, A. Biocompatibility of Resorbable

12
13
14 Polymers: A Historical Perspective and Framework for the Future.

15
16
17
18 *Biomacromolecules* 2019, 20 (4), 1465–1477.

19
20
21
22 <https://doi.org/10.1021/acs.biomac.9b00159>.

23
24
25
26
27
28
29
30
31
32
33
34
35
36
37
38
39 TABLE OF CONTENTS GRAPHIC



50
51 40